BMC Cardiovascular Disorders

RESEARCH

Open Access

Research on noninvasive electrophysiologic imaging based on cardiac electrophysiology simulation and deep learning methods for the inverse problem

Yi Chang[1], Ming Dong[1], Lihong Fan[2*], Bochao Kang[1], Weikai Sun[1], Xiaofeng Li[1], Zhang Yang[1] and Ming Ren[1]

Abstract

Background The risk stratification and prognosis of cardiac arrhythmia depend on the individual condition of patients, while invasive diagnostic methods may be risky to patient health, and current non-invasive diagnostic methods are applicable to few disease types without sensitivity and specificity. Cardiac electrophysiologic imaging (ECGI) technology reflects cardiac activities accurately and non-invasively, which is of great significance for the diagnosis and treatment of cardiac diseases. This paper aims to provide a new solution for the realization of ECGI by combining simulation model and deep learning methods.

Methods A complete three-dimensional bidomain cardiac electrophysiologic activity model was constructed, and simulated electrocardiogram data were obtained as training samples. Particle swarm optimization-back propagation neural network, convolutional neural network, and long short-term memory network were used respectively to reconstruct the cardiac surface potential.

Results The correlation coefficients between the simulation results and the clinical data range from 75.76 to 84.61%. The P waves, PR intervals, QRS complex, and T waves in the simulated waveforms were within the normal clinical range, and the distribution trend of the simulated body surface potential mapping was consistent with the clinical data. The coefficient of determination R^2 between the reconstruction results of all the algorithms and the true value is above 0.80, and the mean absolute error is below 2.1 mV, among which the R^2 of long short-term memory network is about 0.99 and the mean absolute error about 0.5 mV.

Conclusions The electrophysiologic model constructed in this study can reflect cardiac electrical activity, and contains the mapping relationship between the cardiac potential and the body surface potential. In cardiac potential reconstruction, long short-term memory network has significant advantages over other algorithms.

Clinical trial number Not applicable.

Keywords Arrhythmia, Cardiac electrophysiologic imaging, Body surface potential mapping, Deep learning, ECG inverse problem

*Correspondence:
Lihong Fan
lhfan@xjtu.edu.cn

[1]School of Electrical Engineering, Xi'an Jiaotong University, Xi'an 710049, China
[2]The First Affiliated Hospital of Xi'an Jiaotong University, Xi'an 710061, China

Introduction

Arrhythmias are abnormal heart rhythms caused by disorders of the origin and conduction of cardiac activity, which can lead to sudden death, heart failure, and other serious complications. Due to the complexity of risk stratification and prognostic evaluation of cardiac arrhythmias, treatment strategies have to be determined based on the individual condition of patients [1].

The current diagnostic modalities for arrhythmia mainly include invasive and non-invasive diagnostic methods [2]. Invasive diagnostic methods can accurately determine the type of arrhythmia and localize the foci. Common invasive examinations include endocardial labeling, epicardial labeling, and intracavitary electrocardiography [3]. Non-invasive methods include cardiac imaging and electrocardiogram (ECG). The former method is more accurate in the diagnosis of ischemic diseases (e.g., atherosclerotic obstruction or stenosis of the coronary arteries), but is not applicable to other types of cardiac diseases due to certain limitations [4]. ECG can reflect the state of cardiac function in real time to predict and support the diagnosis of cardiovascular diseases. However, the use of fewer lead signals can only provide localized information about cardiac electrical activity, necessitating a higher level of expertise from physicians [5].

In recent years, some scholars have proposed cardiac electrocardiographic imaging (ECGI) technology [6–8]. ECGI can reconstruct cardiac potentials by body surface potential mapping (BSPM) to visualize the propagation of cardiac electrical activity. In comparison to invasive methods, ECGI offers a noninvasive means of reflecting cardiac electrophysiological activity. It allows for efficient and safe screening and identification of patients at high risk for arrhythmias and sudden cardiac death, as well as for localizing arrhythmogenic foci. This is particularly valuable for guiding pre-procedure diagnoses and catheter ablation procedures.

ECGI relies on sufficient data from body surface lead signals and cardiac surface potentials to establish the mapping relationship between the body surface and the heart. Multi-lead ECG systems (the number of leads $\geq$ 64), due to their limited use in clinical practice, rarely provide sufficient data to directly construct a comprehensive database of real lead signals and cardiac surface potentials. Obtaining real cardiac potential data generally requires surgical implantation of cardiac electrodes or catheterization, which is high risk and requires ethical review, hence difficult for clinical application. Consequently, research efforts have concentrated on obtaining simulated lead signals and cardiac potentials using simulation models [9], which is referred to as the ECG forward problem. These simulated data are then employed to establish mapping relationships through regularization methods, as well as machine learning and deep learning techniques [10, 11], a process known as the ECG inverse problem.

The ECG forward problem involves deriving the body surface potential distribution based on the potential distribution and dynamics of the cardiac sources. To accurately solve this problem, it is essential to construct a precise representation of the internal cardiac sources and to define the volume conductor, which includes the visceral organs and the torso. Accurate simulation of human cardiac activity can be used to predict the effects of medical interventions and provide a viable alternative to animal experiments. The results obtained by simulation are close to the real measured signals and can be used as an expansion of the ECG inverse problem dataset. For example, Alday et al. [12]. constructed a complete human torso model containing internal organs and spinal cord based on human magnetic resonance imaging (MRI) images, and inserted the atrial model into the torso model to calculate the distribution of BSPM. Biasi et al. [13]. proposed a new finite-difference method and constructed a three-dimensional (3D) structure of the left ventricle of a specific patient based on medical images for simulating cardiac defibrillation. However, the aforementioned models represent only partial structures of the heart, focusing on either the atria or the ventricles, and do not encompass the complete conduction system. Currently, the state-of-the-art in cardiac modeling computation and simulation is individualized, patient-specific or pathology-specific human cardiac model. These models, although very detailed, are still limited to being ventricular-only [14] or atrial-only [15] models and require significant computational time as well as high-performance software and computers.

The ECG inverse problem aims to extract the relevant parameters of the cardiac source from ECG signals, and construct the cardiac source by comprehensively analyzing the distribution and variations of BSPM, ultimately enabling visualization of the entire cardiac potential. Fundamentally, the ECG inverse problem is a data regression problem of body surface potentials and cardiac potentials [16]. Most traditional solution methods rely on regularization techniques to address the ill-posed nature of the ECG inverse problem, but it is extremely challenging to choose the parameters of these methods [17]. Deep learning outperforms traditional regularization methods in solving inverse problems [18], primarily due to its ability to automatically learn complex data features and mapping relationships, thereby better adapting to diverse inverse problem scenarios. Through end-to-end learning with large-scale training data, deep learning models exhibit stronger generalization capabilities and optimization efficiency, enabling rapid convergence to more accurate solutions. Moreover, the flexible design of

deep learning network architectures allows for superior performance in handling complex textures and details.

In this study, a simplified 3D bidomain electrical activity model was developed to simulate the propagation of cardiac electrical activity. Simulated body surface lead signals and cardiac surface potentials were generated to create a training dataset for the neural network model. The simulation results were then compared with clinical data to validate the model's accuracy. Based on the simulated data of the electrophysiological model, particle swarm optimization-back propagation neural network (PSO-BP), convolutional neural network (CNN), and long short-term memory network (LSTM) were employed respectively to solve the ECG inverse problem and reconstruct cardiac surface potentials. The experimental findings were subsequently validated against clinical data.

Methods

Model construction

The heart-torso bidomain model constructed in this study is an adaptation of the heart model based on the idealized 3D model of Sovilj et al. [19]. The whole model is shown in Fig. 1, which includes a simplified 3D structure of the torso, lungs, and the whole heart (including atria, ventricles, blood chambers, and cardiac fibrous skeleton). The shape and size of the heart in this model are similar to the Visible Human Project gallery of the real human anatomy [20]. The simplified 3D bidomain heart model was simulated using COMSOL Multiphysics (COMSOL AB, Switzerland, v6.0) finite element software. COMSOL allows for the independent import of geometric models, enabling the integration of heart models based on human anatomy for personalized simulation in future studies.

Standard 12-lead (referenced to the Wilson lead system) and body surface 64-lead were placed on the torso surface. Standard and augmented lead signals were obtained from 4 electrodes (V_R, V_L, V_F, V_{GND}) at the limbs, and precordial lead signals were obtained from 6 electrodes (V_1-V_6) on the anterior chest wall. In addition, 64-lead electrodes were placed on the front and back side of the torso to obtain body surface potentials. The arrangement consists of 32 electrodes on both the front and back surfaces (V_{64_i}, where i represents the lead number ranging from 1 to 64), as indicated by the dark gray dots in Fig. 1a. The standard 12-lead ECG is defined in accordance with the literature [19], and 64-lead signals are the difference between the lead electrode potentials and Wilson central terminal.

Considering the volume conductor effect, the conductivity and permittivity of each model component are assigned in accordance with the actual measured values of human tissues [21]. For the volume conductor region, the extracellular voltage V is controlled by the Laplace Eq.

$$\nabla \cdot (-\sigma_0 \nabla V) = 0 \tag{1}$$

where σ_0 is the conductivity of torso, lungs, blood chambers, and fibrous skeleton. The values of conductivity and permittivity of each model subdomain are given in Table 1.

The cardiac model is divided into seven regions based on cellular properties and tissue conductivity: sinoatrial node (SAN), atria, atrioventricular node (AVN), His bundle, bundle branches (BNL), Purkinje fibers, and ventricles. The ventricles and atria are separated by fibrous skeleton and only connected by the AVN.

Cardiac electrical activity is characterized by the modified FitzHugh-Nagumo model [22], which utilizes three

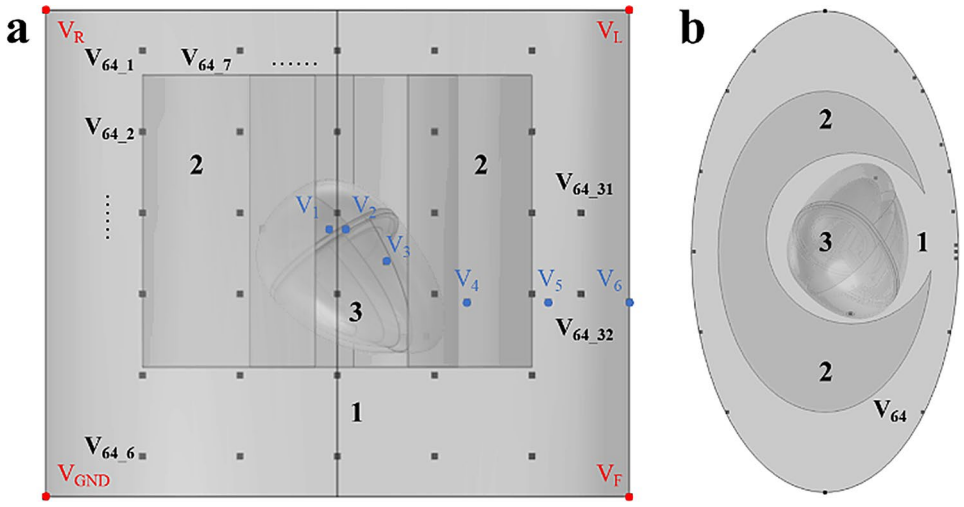

Fig. 1 3D geometry of the heart-torso model. 1 = torso, 2 = lungs, 3 = heart. (**a**) Frontal view. (**b**) Top view

Table 1 Conductivity and permittivity settings for model subdomains

Subdomain	Conductivity(S/m)	Permittivity
Heart	0.053677	23,562,000
Fibrous skeleton	10^{-9}	10^{9}
Blood chambers	0.7	5260
Lungs	0.038904	32,248,000
Torso	0.20197	25,700,000

dependent variables to depict the cardiac cell activation process at the cellular level: V_e for the extracellular potential, V_i for the intracellular potential, and u for the recovery variable that reflects the refractory period. The formula is given in Eq. (2) and Eq. (3).

$$\begin{aligned} \frac{\partial V_e}{\partial t} - \frac{\partial V_i}{\partial t} + \nabla \cdot (-\sigma_e \nabla V_e) &= i_{ion,l} \\ \frac{\partial V_i}{\partial t} - \frac{\partial V_e}{\partial t} + \nabla \cdot (-\sigma_i \nabla V_i) &= -i_{ion,l} \\ \frac{\partial u}{\partial t} &= ke\left[\frac{(V_m - B)}{A} - du - b\right] \end{aligned} \tag{2}$$

$$\begin{aligned} i_{ion,1} &= kc_1 (V_m - B)\left(a - \frac{V_m - B}{A}\right)\left(1 - \frac{V_m - B}{A}\right) \\ &\quad + kc_2 u \\ i_{ion,2} &= kc_1 (V_m - B)\left(a - \frac{V_m - B}{A}\right)\left(1 - \frac{V_m - B}{A}\right) \\ &\quad + kc_2 u (V_m - B) \end{aligned} \tag{3}$$

where σ_e and σ_i are the extracellular and intracellular conductivity, respectively. $V_m = V_i - V_e$ is the transmembrane potential (TMP). a, A and B are used to control the threshold of the cellular action potential. c_1, c_2 and k are the unit conversion factor. b, d and e are used to regulate the rate of change of the recovery variable, reflecting the duration of the cellular action potential. $i_{ion,l}$ is the membrane ion flow, where $l = 1$ represents the membrane ion flow in the SAN, and $l = 2$ represents other regions.

The region-specific parameters for each region are given in Table 2 to reflect electrophysiological differences. These parameters are based on the work presented in the literature [19] and have been adjusted accordingly to fit the present simulation model. For example, the values of a and b in the SAN differ from those in other regions, reflecting its unique function in the autonomous generation of electrical activation. This characteristic is also evident in the action potential thresholds A and B, which are unique to the SAN compared to other regions. σ_e and σ_i of the AVN is used to simulate its lower conduction properties.

The complete mesh of the generated finite element mesh contained 58,151 domain cells, 13,074 boundary cells, and 1290 edge cells. The simulation was performed on an Intel Core i9-12900 K workstation with a processing power of approximately 35.58 TFLOPS. The simulation takes about 3 h to calculate 1200 ms of cardiac activity with 1 ms resolution.

Cardiac potential reconstruction

The clinical ECG aims to extract the relevant parameters of the cardiac source from the standard 12-lead signals. Additionally, the ECG inverse problem aids in constructing the cardiac source by comprehensively analyzing the distribution and variations of BSPM, ultimately enabling visualization of the entire cardiac potential. Fundamentally, the ECG inverse problem is a data regression problem of body surface potentials and cardiac potentials. The mapping relationship between cardiac potentials and body surface potentials is usually defined according to [16]

$$Y = TX + N \tag{4}$$

where Y is the body surface potential, T is the transfer coefficient matrix, X is the cardiac surface potential, and N is the noise.

The ECG inverse problem is considered ill-posed, meaning that small disturbances in the data can lead to significant errors in the resulting solutions. Most traditional solution methods rely on regularization techniques to address the ill-posed nature of the ECG inverse problem. Common regularization methods include Tikhonov

Table 2 Region-Specific parameters of the cardiac conduction system

Parameter	SAN [a]	Atria	AVN [b]	His	BNL [c]	Purkinje	Ventricles
a	-0.6	0.13	0.13	0.13	0.13	0.13	0.13
b	-0.3	0	0	0	0	0	0
c_1 ($A{\cdot}s{\cdot}V^{-1}{\cdot}m^{-3}$)	1000	2.6	2.6	2.6	2.6	2.6	2.6
c_2 ($A{\cdot}s{\cdot}V^{-1}{\cdot}m^{-3}$)	1	1	1	1	1	1	1
d	0	1	1	1	1	1	1
e	0.0489	0.0158	0.0132	0.013	0.0037	0.0056	0.0065
k (s^{-1})	1000	0.4	1	1	1	1	1
A (V)	0.033	0.14	0.14	0.14	0.14	0.14	0.14
B (V)	-0.022	-0.085	-0.085	-0.085	-0.085	-0.085	-0.085
$\sigma_e\ (mS \cdot m^{-1})$	0.75	20	2.5	25	7.5	17.5	4
$\sigma_i\ (mS \cdot m^{-1})$	0.75	20	2.5	25	7.5	17.5	4

[a] SAN = sinoatrial node, [b] AVN = atrioventricular node, [c] BNL = bundle branches

regularization and the L-curve method [8]. While these approaches can be as effective as more advanced methods for regularization under real fibrillation conditions, selecting the appropriate regularization parameters can be quite challenging. Even minor adjustments to these parameters can significantly impact the reconstruction performance of cardiac potentials [17].

Other methods, such as generalized singular value decomposition (GSVD) [23] and spatiotemporal regularization (STRE) [24], also be employed to solve the ECG inverse problem. However, these approaches are often influenced by systematic noise, particularly geometric noise, which can result in suboptimal reconstruction of cardiac potential and reduced generalizability. These limitations render them inapplicable for the solution of personalized models.

In recent years, machine learning and deep learning have developed rapidly, demonstrating higher computational efficiency and enhanced generalization performance in solving ECG inverse problems. In this study, we utilized a dataset obtained from simulations of the cardiac EP model to employ particle swarm optimization-back propagation neural network (PSO-BP) [25], convolutional neural network (CNN) [26], and long short-term memory (LSTM) [27] to solve the ECG inverse problem. We compared the reconstruction performance of these different methods. Details of the algorithms, including model structures and parameters, are provided in the supplementary file. The experimental conclusions were further validated using the clinical dataset exported by ECGsim, which was obtained through Carto system [28].

Data pre-processing and evaluation

The simulation data of the cardiac EP model described earlier was used to train the deep learning network models. The 1000 ms of simulated data was sampled at 1 ms intervals, resulting in 1000 sets of sample data. From this dataset, we selected 1 ms of data every 5 ms, yielding a total of 200 test samples, while the remaining 800 sets comprised the training samples. For the clinical dataset, data from the first 5 heartbeat cycles were used for model training and the 6th heartbeat cycle was designated for testing.

To assess the impact of the two dataset division methods on model performance, a pre-experiment was conducted using LSTM networks. For the clinical dataset, we used the above two dataset division methods (i.e., sampling at equal time intervals and dividing by heartbeat cycles) respectively. The results indicated that the model output error was not significantly different between these two methods, with both errors being below 0.5 mV. Given that the simulated dataset contained fewer heartbeat cycles, equal time interval sampling was employed to better capture the information from different segments of the ECG data. In future studies, when sufficient ECG data are available, the method of dividing by heartbeat cycles is recommended.

In order to make the model more robust, the following preprocessing works were performed on the body surface potential data:

(1) Add 15dB Gaussian noise to simulate the noise influence on the clinical data, which can improve the generalization performance and effectiveness of the algorithm.

(2) Use normalization operation to scale the feature values, which can avoid the difficulty of model training caused by excessive data differences.

The coefficient of determination R^2 and mean absolute error (MAE) are used to quantitatively assess the accuracy of reconstructing the TMP. The calculation formulas are defined according to

$$R^2 = 1 - \frac{\sum_{i=1}^{n}(y_i - \widehat{y}_i)^2}{\sum_{i=1}^{n}(y_i - \bar{y})^2} \tag{5}$$

$$MAE = \frac{1}{n}\sum_{i=1}^{n} |\widehat{y}_i - y_i| \tag{6}$$

where y_i is the true value of cardiac TMP, $\widehat{y}_i$ is the mean value of TMP, and $\bar{y}_i$ is the predicted value of TMP.

Results

Simulation results

Figure 2 illustrates a visualization image of the cardiac electrical conduction activity within a single sinus rhythm. The SAN, atria, AVN, His bundle, BNL, Purkinje fibers, and ventricles are depolarized (from low to high potentials) and repolarized (from high to low potentials) sequentially based on the order of electrical activation propagation.

At 10th ms, electrical activation is generated in the SAN located in the right atrium at the upper left of the image (brighter part). At 50th ms, the electrical activation begins to conduct along the atrial wall and reaches the AVN at 80th ms, stimulating the AVN and His bundle to conduct action potentials. At 105th ms, the electrical activation begins to conduct along the right and left BNL and reaches the Purkinje fibers at 125th ms. During the period of 145–180 ms, Purkinje fibers conducts electrical activation, which causes the depolarization of the left and right ventricles. Subsequently each part of the conduction system completes repolarization according to the sequence of depolarization. For example, the repolarization occurs in the BNL and Purkinje fibers at 220th ms and 245th ms, respectively. During the period of 260–290 ms, the ventricles has completed the repolarization. The conduction sequence of simulation model is consistent

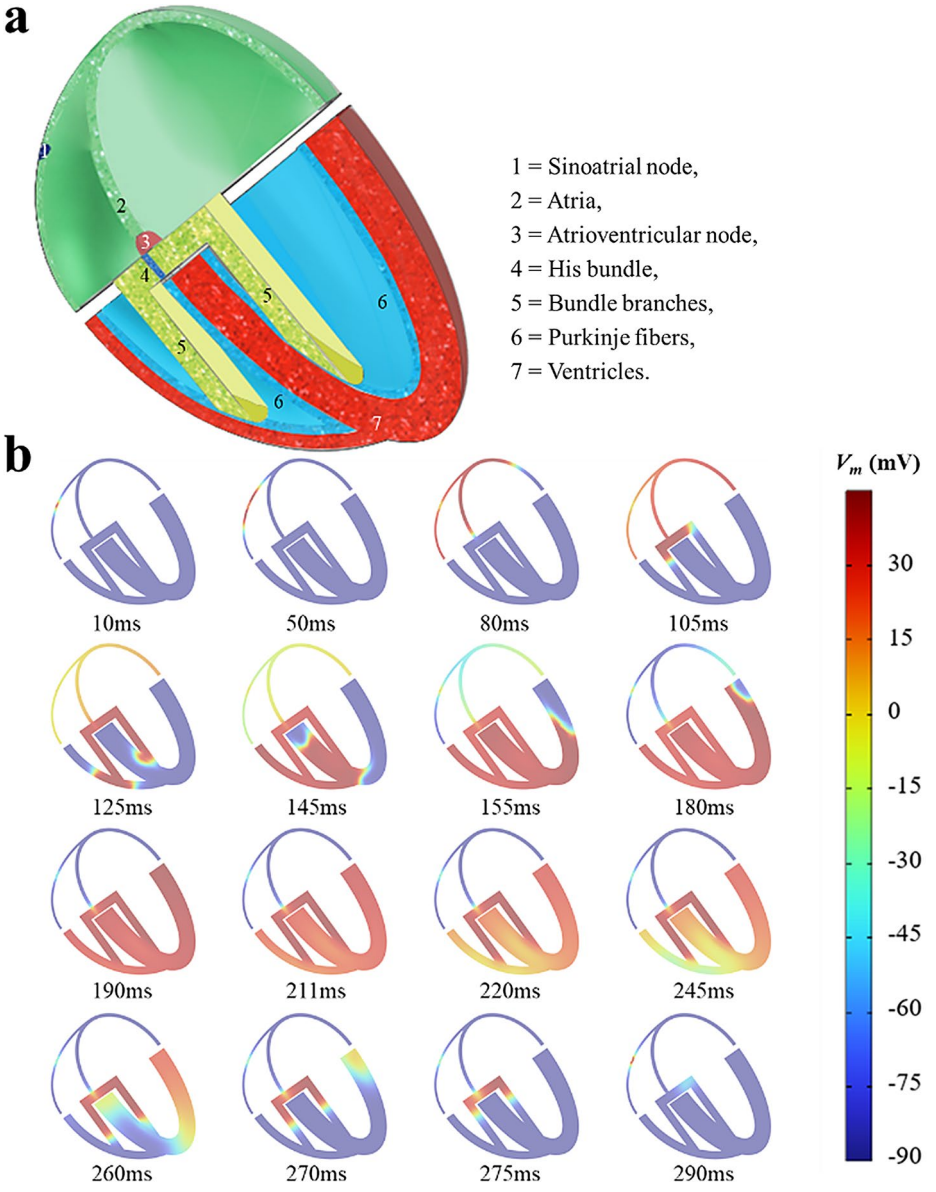

Fig. 2 Sequence of cardiac electrical activation at different time. (**a**) Conduction system. (**b**) Conduction sequence

with that of human heart [29], which confirms the validity of the improved model.

Figure 3 illustrates the 64-lead ECG waveforms of a complete heartbeat cycle obtained from the simulation, with the anterior 32-lead signals in Fig. 3(a) and the posterior 32-lead signals in Fig. 3(b). The vertical calipers in the figure mark the start and end points of the detected QRS wave complex. The amplitude of anterior lead signals is slightly larger than that of posterior lead signals. The differences between the anterior and posterior leads reflect the influence of the lungs on the conduction of the cardiac activity.

In addition, 196 nodes on the cardiac surface were selected to obtain TMP, including 68 atrial nodes and 128 ventricular nodes. The acquired cardiac potentials combined with the 64-lead signals described above can be used to study the ECG inverse problem.

Model validation

ECG comparison

To verify the validity of the improved model, the simulated ECG obtained from the EP model are compared with the clinical ECG. The clinical ECG are acquired from 47 samples from the MIT-BIH arrhythmia database. The database utilized in this study contains only two lead signals per sample, and the types of leads are inconsistent across samples. Specifically, the majority of samples include leads V_{II} and V_5, while a smaller number of samples consist of leads V_{II} and V_1 or V_{II} and V_2. Two records of each lead are selected for comparison with

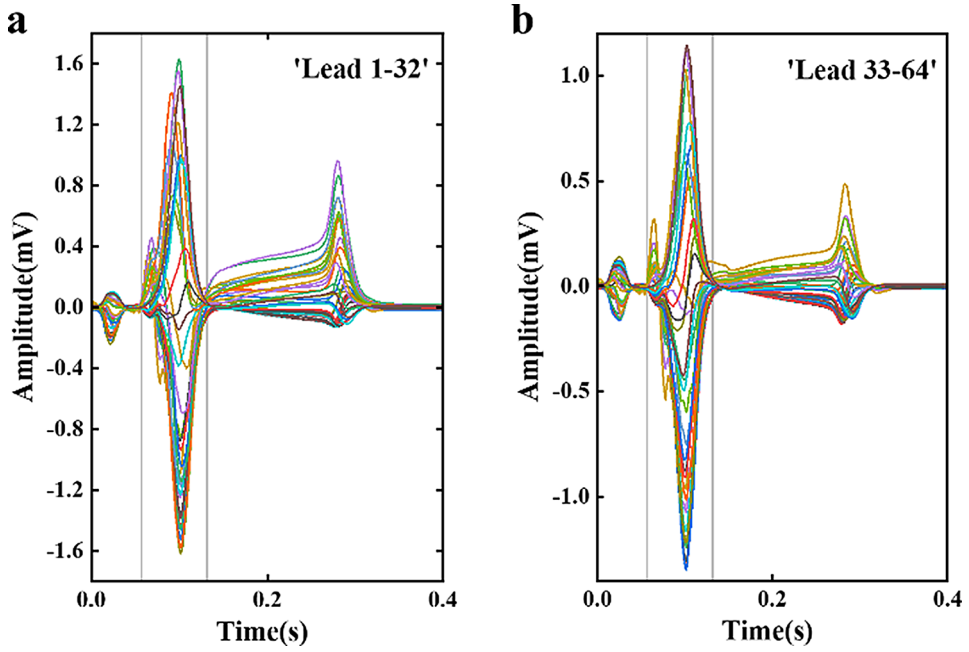

Fig. 3 ECG of the body surface 64-lead signals. (**a**) The anterior 1–32 lead signals. (**b**) The posterior 33–64 lead signals

the simulation results in this paper. The clinical data of V_{II} are from records 100 and 103, V_1 from 105 to 116, V_2 from 103 to 172, and V_5 from 100 to 114. Figure 4 presents the waveforms of the simulation data, along with the range of variation over multiple cycles of the clinical data and the average values.

The correlation coefficients between the simulation results and the mean values of clinical data range from 75.76 to 84.61%, and the trends of waveform changes are consistent. The results show that the cardiac electrophysiological simulation model established in this paper is in general agreement with the clinical data. It should be noted that there are still some differences between simulated and real ECG signals, which are related to the idealized settings of the cardiac model. For example, the model simplified the atrial structure as well as the Purkinje net and did not perform myocardial fiber orientation.

The purpose of our study is to expand the ECG dataset needed to solve the ECG inverse problem. As shown in the comparison with the clinical data, the model constructed in this study can reflect cardiac electrical activity, and contains the mapping relationship between the cardiac potential and the body surface potential.

BSPM comparison

Body surface labeling techniques generally reconstruct cardiac potentials via BSPM, hence simulated BSPM and clinical BSPM are also compared. Clinical BSPM is obtained from patient data collected by Thomas Berger (Department of Internal Medicine, Division of Cardiology, Medical University Innsbruck, Innsbruck, Austria) et al. [28].

The structural similarity (SSIM) is commonly applied to evaluate the consistency of two types of data. SSIM can measure the picture distortion as well as the similarity between two pictures. Unlike mean square error (MSE) and peak signal-to-noise ratio (PSNR), which measure absolute error, SSIM is a perceptual model that is more consistent with the human visual system. SSIM considers three key features of a picture: luminance $l(a,b)$, contrast $c(a,b)$, and structure $s(a,b)$, which are defined according to

$$\begin{aligned} l(a,b) &= (2\mu_a\mu_b + C_1)/(\mu_a^2 + \mu_b^2 + C_1) \\ c(a,b) &= (2\sigma_a\sigma_b + C_2)/(\sigma_a^2 + \sigma_b^2 + C_2) \\ s(a,b) &= (\sigma_{ab} + C_3)/(\sigma_a\sigma_b + C_3) \end{aligned} \tag{7}$$

where μ_a and μ_b represent the mean of image a and image b. σ_a and σ_b represent the standard deviation of each image, σ_{ab} is the covariance of the two images, and C_1, C_2, and C_3 are scalar constants. Combining these three features, SSIM is defined according to

$$SSIM\,(a,b) = [l(a,b)]\,[c(a,b)]\,[s(a,b)] \tag{8}$$

The mean SSIM (MSSIM) is used to assess the degree of similarity between the clinical data and the simulated data, which is defined according to

$$MSSIM(A,B) = \frac{1}{M}\sum_{i=1}^{M} SSIM(a_i,b_i) \tag{9}$$

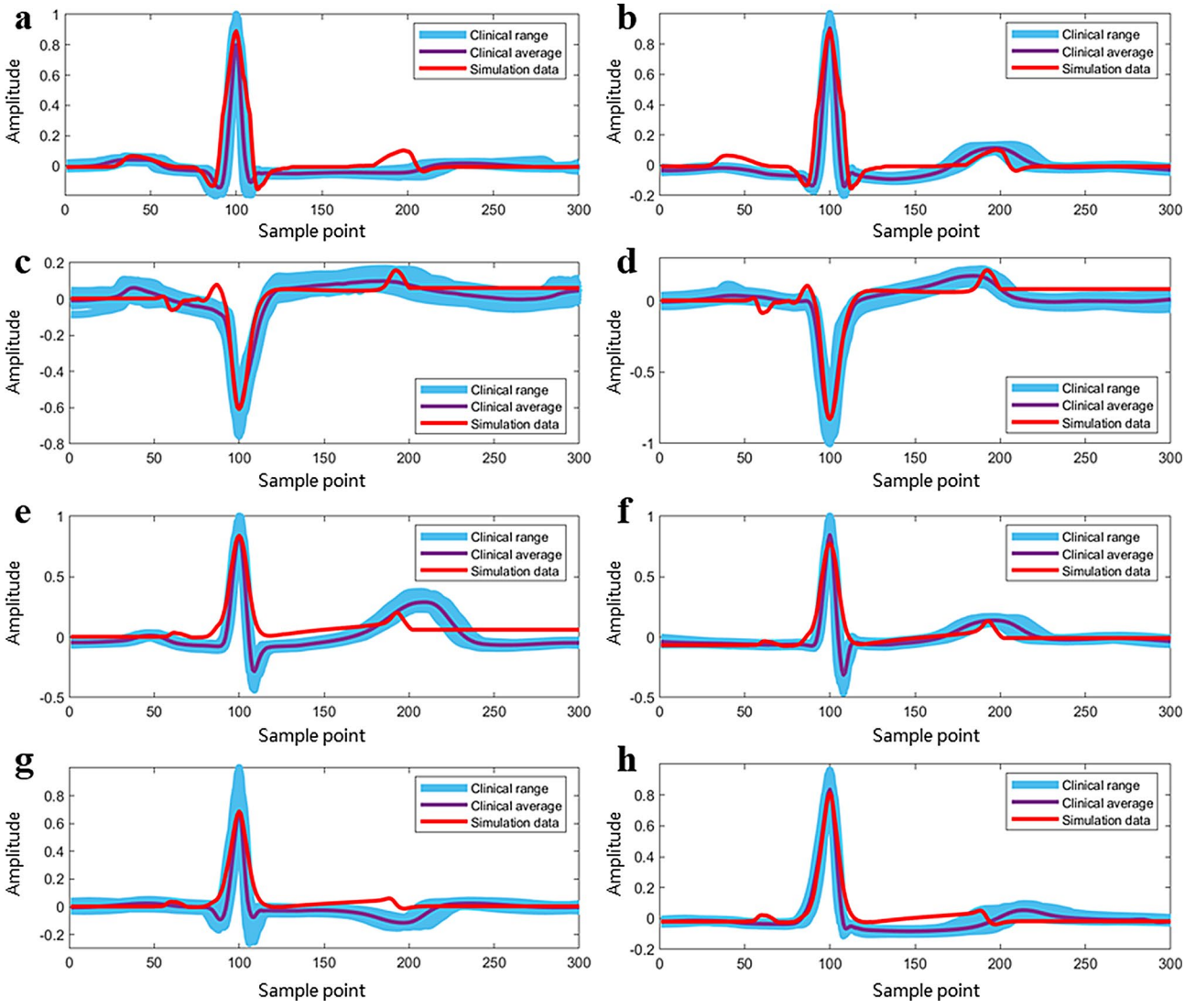

Fig. 4 Comparison of simulation results with ECG database. V_{li}: Records 100 (**a**) and 103 (**b**). V_1: Records 105 (**c**) and 116 (**d**). V_2: Records 103 (**e**) and 172 (**f**). V_5: Records 100 (**g**) and 114 (**h**)

where A and B are the reference and comparison images, respectively, a_i and b_i are the image contents of the i^{th} localized window, and M is the number of localized windows of the image.

Figure 5 illustrates the clinical and simulated BSPM corresponding to the moments when the ECG R-wave reached the peak, representing the distribution of the body surface potential during the ventricular depolarization period. The location of the heart is the lower left side at the middle of the whole labeling map. During the ventricular depolarization, the maximum values of the body surface potential are all located near the left chest wall, while the minimum values are located on the right wall of the torso, demonstrating a distinct trend of bipolar distribution.

The MSSIM between the clinical and simulated BSPM shown in Fig. 5 is 0.743, calculated with a window size of 11×11 pixels. This value indicates that the simulation results of the cardiac EP model are similar to the potential distribution of the clinical data, and the distribution trend is consistent. The above results demonstrate that the simulated BSPM can be used to analyze the process of cardiac electrical activity, and obtain the corresponding parameters.

TMP reconstruction of different datasets

TMP reconstruction based on simulated data

The results of TMP reconstruction at each node of the cardiac model are similar, and node 125 is chosen for illustration in this study, as shown in Fig. 6.

The TMP reconstructed by PSO-BP has slight fluctuations, and the potential amplitudes reconstructed by 1D-CNN and 2D-CNN are more obviously different from the true value, but all the depolarization and

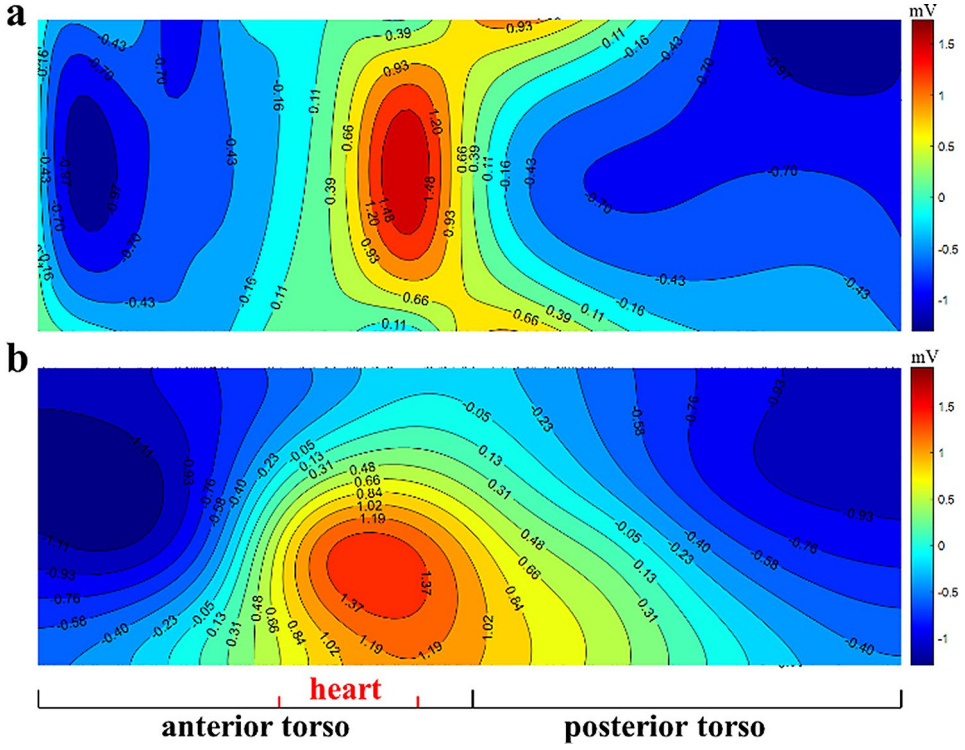

Fig. 5 Comparison of (**a**) the clinical BSPM and (**b**) the simulated BSPM

repolarization times basically match the true value (the difference is less than 5%), and the trend of the three TMPs are consistent with the true value. The TMP reconstructed by LSTM coincides with the true value.

To quantitatively evaluate the results of the reconstruction of cardiac potential, the cardiac surface is divided into four regions based on the distribution of node locations, including left atrium (LA), right atrium (RA), left ventricle (LV), right ventricle (RV). The results of the TMP reconstruction are evaluated separately for each region, as shown in Table 3; Fig. 7.

For the four cardiac potential reconstruction regions, the average values of R^2 between the output values of all the algorithms and the true values are above 0.80, and the MAE are below 2.1 mV, where the R^2 of LSTM can be reached to 0.99, and the MAE is less than 0.5 mV. The training duration of PSO-BP, 1D-CNN, 2D-CNN, and LSTM are 0.34, 1.14, 1.13, and 0.29 h, respectively. The reconstruction results suggest that LSTM is obviously more appropriate for solving the ECG inverse problem.

TMP reconstruction based on clinical data

Table 4 presents the training duration and the quantitative indicators of TMP reconstruction based on clinical patient data. Since the various cardiac regions are barely delineated in the clinical data, only the overall reconstruction results are given, without separate statistics for each region.

To better visualize the performance of the four methods, cardiac TMP electrograms and isopotential lines at five moments, 99th ms, 234th ms, 284th ms, 309th ms, and 330th ms, are plotted for imaging, as shown in Fig. 8.

Obviously, the cardiac TMP reconstructed by LSTM method is closer to the real potential distribution than the other methods. The results indicate that LSTM is superior to the first three methods in reconstructing cardiac TMP, agreeing with the conclusions from the simulated data.

Discussion

Further applications of EP modeling

In this study, a complete 3D bidomain cardiac activity model was constructed for simulating the conduction process of cardiac electrical activity, and 64-lead electrodes were set on the body surface to obtain the body surface potential signals. Different from the existing specialized ECG positive problem simulation software (e.g., ECGsim), the cardiac EP model constructed has a complete cardiac electrical activity conduction system. By varying the electrophysiological parameters and voltage-current control equations, more realistic cardiac diseases such as myocardial infarction and atrial fibrillation can be simulated [30]. As Sovilj et al. [19]. simulated the occurrence of myocardial infarction by setting the infarct zone (conductivity and electrical excitation conduction coefficient were set to 0), the ST segments of the simulated

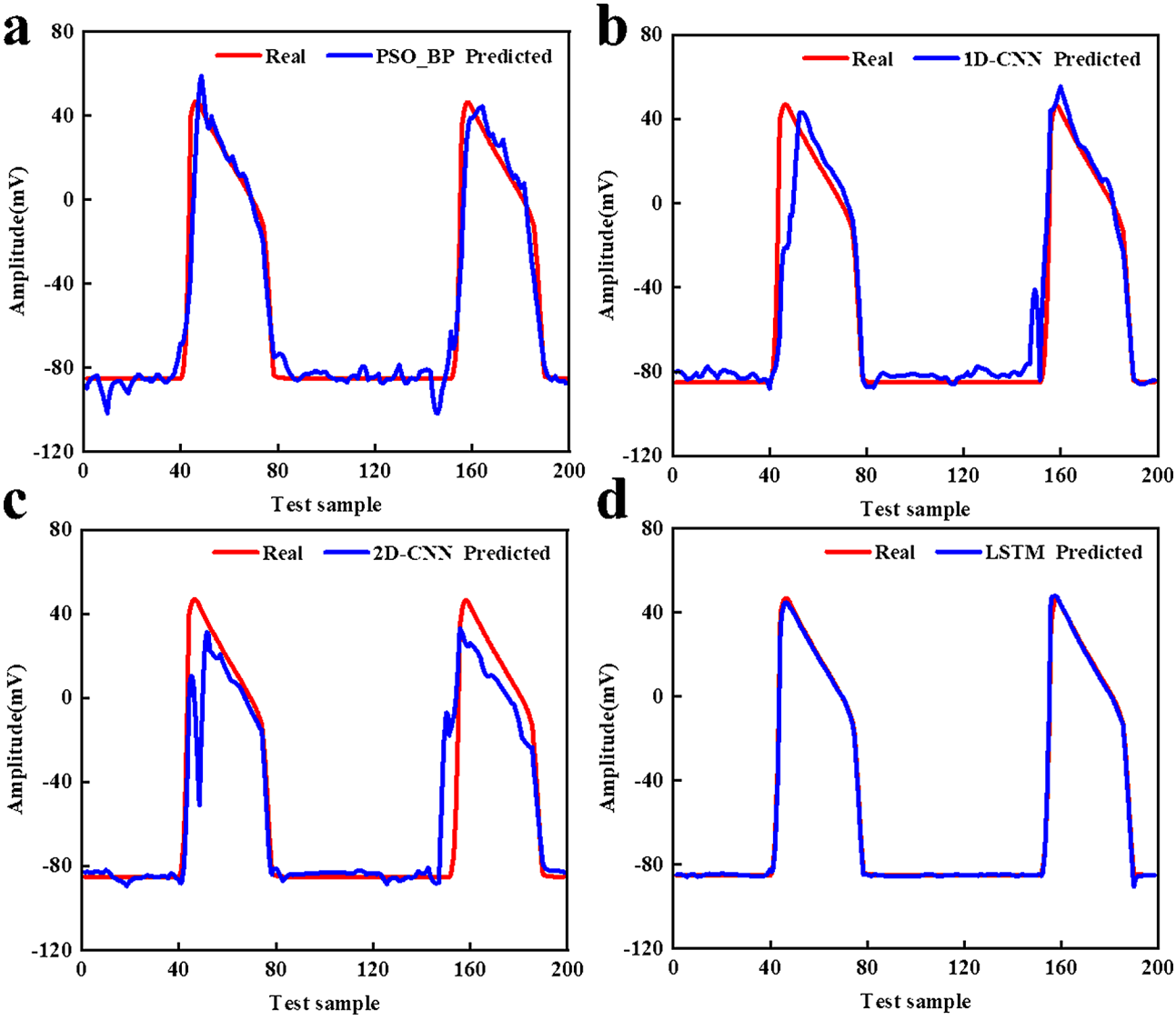

Fig. 6 Comparison of reconstructed TMP with real waveforms. (**a**) Particle swarm optimization-back propagation neural network (PSO-BP). (**b**) One-dimensional convolutional neural network (1D-CNN). (**c**) Two-dimensional convolutional neural network (2D-CNN). (**d**) Long short-term memory network (LSTM)

Table 3 Results of TMP reconstruction of cardiac surface for 8 regions by 4 methods

		PSO-BP [a]	1D-CNN [b]	2D-CNN [c]	LSTM [d]
LA	R^2 [e] (%)	93.2 ± 1.40	94.4 ± 0.64	94.3 ± 0.66	96.9 ± 0.40
	MAE [f] (mV)	1.00 ± 0.14	0.75 ± 0.05	0.73 ± 0.05	0.40 ± 0.04
RA	R^2 (%)	85.0 ± 3.80	96.0 ± 0.30	95.2 ± 0.40	96.6 ± 0.35
	MAE (mV)	1.57 ± 0.23	0.70 ± 0.04	0.72 ± 0.05	0.45 ± 0.06
LV	R^2 (%)	84.6 ± 3.80	98.5 ± 0.44	98.6 ± 0.58	99.7 ± 0.11
	MAE (mV)	1.88 ± 0.17	0.86 ± 0.40	0.54 ± 0.08	0.22 ± 0.05
RV	R^2 (%)	90.0 ± 0.90	98.3 ± 0.41	98.7 ± 0.26	99.8 ± 0.03
	MAE (mV)	1.57 ± 0.11	0.66 ± 0.04	0.51 ± 0.04	0.19 ± 0.03

[a] PSO-BP = Particle swarm optimization-back propagation neural network, [b] 1D-CNN = One-dimensional convolutional neural network, [c] 2D-CNN = Two-dimensional convolutional neural network, [d] LSTM = Long short-term memory network, [e] R^2 = The coefficient of determination, [f] MAE = The mean absolute error

waveforms appeared to change in accordance with the clinical case. Alday et al. [12]. simulated the activity of atrial ectopic foci by applying different cycles of electrical pulse stimulation to the atria in order to study the changes in P-wave morphology caused by rapid atrial arrhythmias, such as atrial tachycardia and atrial fibrillation. Given the relatively scarce available clinical datasets, in future studies, we could consider providing more abundant training samples for the ECG inverse problem by modeling the occurrence of various types of cardiovascular diseases.

Performance of deep learning

Based on the constructed cardiac EP model, the simulated data were used as the training samples for the

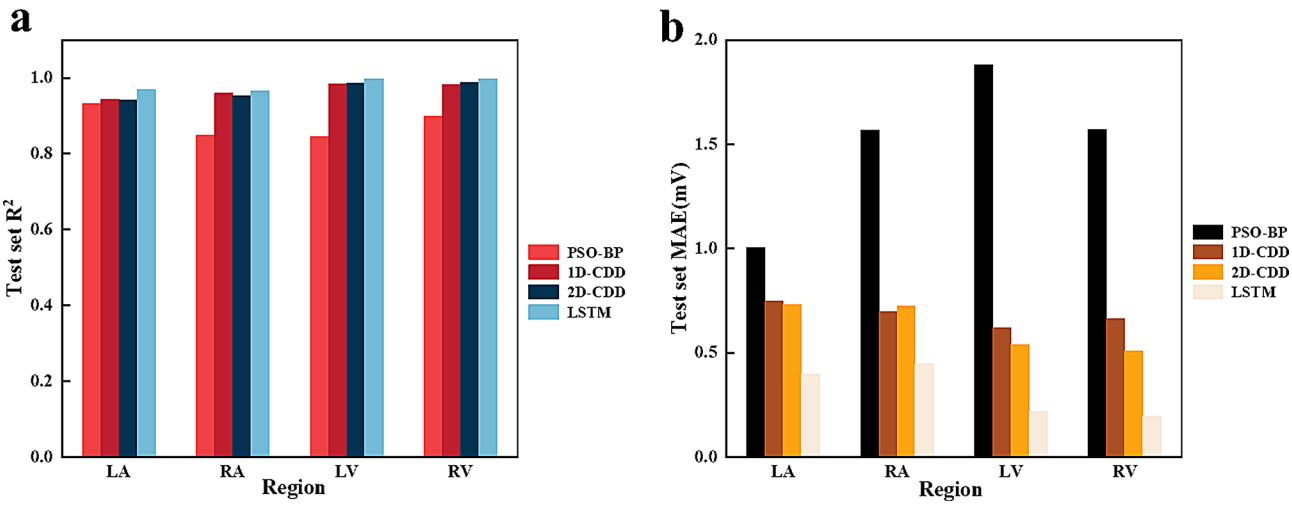

Fig. 7 Quantitative analysis of reconstruction results and true values. (**a**) The mean value of the coefficient of determination (R^2) for each region. (**b**) The mean value of the mean absolute error (MAE) for each region. PSO-BP = Particle swarm optimization-back propagation neural network, 1D-CNN = One-dimensional convolutional neural network, 2D-CNN = Two-dimensional convolutional neural network, LSTM = Long short-term memory network

Table 4 Training duration and TMP reconstruction results based on clinical data

	PSO-BP [a]	1D-CNN [b]	2D-CNN [c]	LSTM [d]
Duration (h)	5.8	2.2	1.9	1.4
R^2 (%)	92.5 ± 3.2	92.1 ± 4.5	96.8 ± 1.6	97.5 ± 1.2
MAE (mV) [e]	3.01 ± 0.79	2.07 ± 0.23	1.48 ± 0.16	1.20 ± 0.13

[a] PSO-BP = Particle swarm optimization-back propagation neural network, [b] 1D-CNN = One-dimensional convolutional neural network, [c] 2D-CNN = Two-dimensional convolutional neural network, [d] LSTM = Long short-term memory network

neural network. The PSO-BP, 1D-CNN, 2D-CNN, and LSTM were used respectively to reconstruct the cardiac potentials, and the experimental conclusions were validated with clinical datasets. The R^2 between the reconstruction results of all the algorithms and the true value is above 0.80, and the MAE is below 2.1 mV. The R^2 of LSTM is about 0.99 and MAE about 0.5 mV, suggesting that LSTM has the best performance in the cardiac potential reconstruction. The cardiac electrical signals have physiological properties and exhibit patterns of change over time. LSTM is efficient at processing the relationships between temporal signals due to its ability to learn long-term dependencies in sequence data. This capability may explain why LSTM is well-suited for reconstructing cardiac potentials.

Limitations

The bidomain cardiac activity model constructed in this paper has idealized and simplified the geometric model of the cardiac conduction system and torso, which may impact the accuracy and reliability of the model in simulating real clinical scenarios. For example, the geometry of the bundle branches is different from the real anatomical structure (combining left anterior and left posterior branches into a single bundle), which may result in the inability to accurately differentiate between left anterior and left posterior bundle branches block. The lack of fiber orientation and the simplification of the Purkinje net in the cardiac structure can affect the generation of ECG signals. This is one of the factors contributing to the differences observed between simulated and real ECG signals. The simplification of the torso may also lead to inconsistencies between the simulated lead sites and the clinical locations. In addition, only cardiac electrical activity conduction is simulated in this paper, which does not involve the cardiac mechanical motion as well as electromagnetic coupling. A limited number of simulation datasets and data types may also lead to overfitting. Therefore, in future studies, we can consider further optimizing the complexity of the model, extracting cardiac medical imaging data to establish a geometric model and simulating the multimodal activities of the heart through the coupling of multiple physical fields, so as to improve the reliability and operability of the model in clinical practice.

Conclusions

Compared with traditional 12- or 18-lead, ex vivo electrophysiology imaging can provide more abundant cardiac information. Compared with invasive diagnostic methods, it can provide a safe and non-invasive approach for health monitoring, favoring the screening and identification of patients at high risk of cardiac diseases. Using deep learning technology to solve the ECG inverse problem, with less computational cost and shorter training duration, the visualization of cardiac potentials can be achieved rapidly and efficiently, which is of great

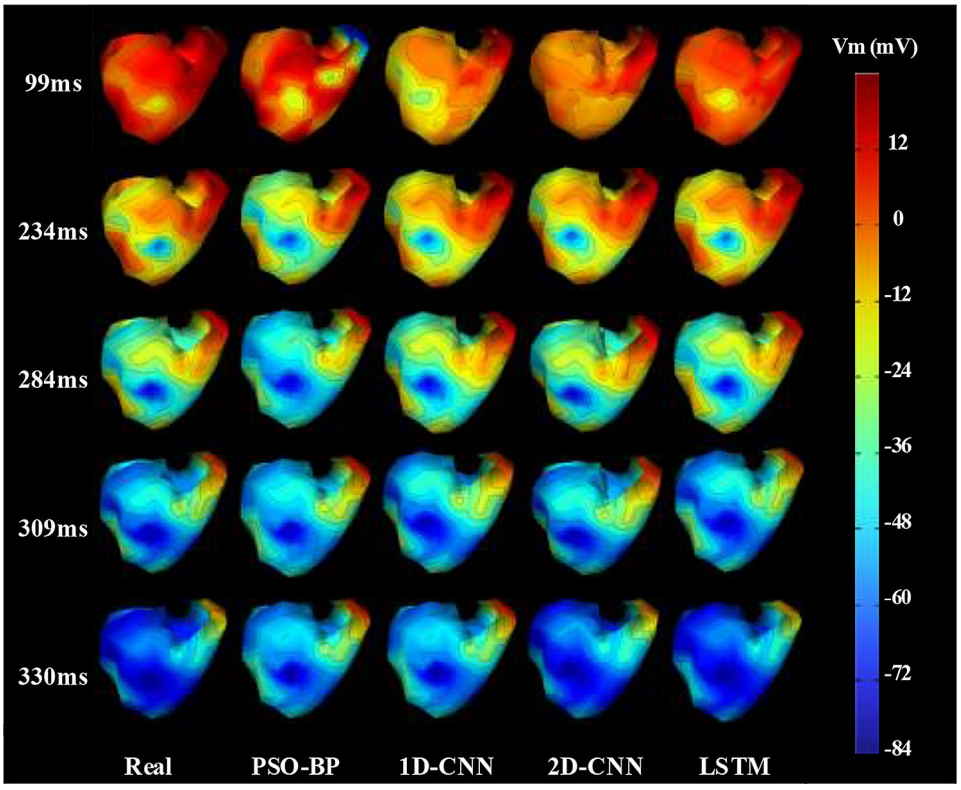

Fig. 8 Comparison of reconstructed TMP with real values at 5 time points

significance for guiding the pre-operative diagnosis as well as catheter ablation procedures.

Abbreviations

3D	Three-dimensional
AVN	Atrioventricular node
BNL	Bundle branch
BSPM	Body surface potential mapping
CNN	Convolutional neural network
ECG	Electrocardiogram
ECGI	Electrocardiographic imaging
EP	Electrophysiology
GSVD	Generalized singular value decomposition
LA	Left atrium
LSTM	Long short-term memory network
LV	Left ventricle
MAE	Mean absolute error
MRI	Magnetic resonance imaging
MSE	Mean square error
MSSIM	Mean structural similarity
PSNR	Peak signal-to-noise ratio
PSO-BP	Particle swarm optimization-back propagation neural network
RA	Right atrium
RV	Right ventricle
SAN	Sinoatrial node
SSIM	Structural similarity
STRE	Spatiotemporal regularization
TMP	Transmembrane potential

Supplementary Information

The online version contains supplementary material available at https://doi.org/10.1186/s12872-025-04728-2.

Supplementary Material 1

Acknowledgements
Not applicable.

Author contributions
Y.C. built the simulation model and deep learning model, and was a major contributor in writing the manuscript. M.D. conceived the study concept and designed the experimental plan. L.F. performed the data analysis and clinical validation. W.S. revised the manuscript. X.L. and Z.Y. generated figures and visualization of the results. B.K. conducted deep learning model training. M.R. Guided the design and optimization of experimental plan. All authors read and approved the final manuscript.

Funding
The study was supported by the National Natural Science Foundation of China under Grants 62176208.

Data availability
The datasets generated and/or analyzed during the current study are available in the MIT-BIH arrhythmia database repository, https://archive.physionet.org/cgi-bin/atm/ATM.

Declarations

Ethics approval and consent to participate
The study was approved by the Ethical Committee of Xi'an Jiaotong University.

Consent for publication
Not applicable.

Competing interests
The authors declare no competing interests.

Received: 17 January 2024 / Accepted: 2 April 2025
Published online: 28 April 2025

References

1. Antzelevitch C, Burashnikov A. Overview of basic mechanisms of cardiac arrhythmia. Card Electrophysiol Clin. 2011;3(1):23–45.
2. Takase B, Ikeda T, Shimizu W, Abe H, Aiba T, Chinushi M et al. JCS/JHRS 2022 guideline on diagnosis and risk assessment of arrhythmia. Circ J. 2023; cj–22.
3. Fang L, Xu J, Hu H, Chen Y, Shi P, Wang L, et al. Noninvasive imaging of epicardial and endocardial potentials with low rank and sparsity constraints. IEEE Trans Biomed Eng. 2019;66(9):2651–62.
4. Paddock S, Tsampasian V, Assadi H, Mota BC, Swift AJ, Chowdhary A, et al. Clinical translation of three-dimensional Scar, diffusion tensor imaging, four-dimensional flow, and quantitative perfusion in cardiac MRI: A comprehensive review. Front Cardiovasc Med. 2021;8:682027.
5. Bonomini MP, Villarroel-Abrego H, Garillo R. Spatial variance in the 12-lead ECG and mechanical dyssynchrony. J Interv Card Electrophysiol. 2021;62(3):479–85.
6. Ramanathan C, Jia P, Ghanem R, Calvetti D, Rudy Y. Noninvasive electrocardiographic imaging (ECGI): application of the generalized minimal residual (GMRes) method. Ann Biomed Eng. 2003;31(8):981–94.
7. Rudy Y. Noninvasive ECG imaging (ECGI): mapping the arrhythmic substrate of the human heart. Int J Cardiol. 2017;237:13–4.
8. Salinet J, Molero R, Schlindwein FS, Karel J, Rodrigo M, Rojo-Álvarez JL, et al. Electrocardiographic imaging for atrial fibrillation: a perspective from computer models and animal experiments to clinical value. Front Physiol. 2021;12:653013.
9. Laubenbacher R, Mehrad B, Shmulevich I, et al. Digital twins in medicine[J]. Nat Comput Sci. 2024;4(3):184–91.
10. Lan S, Li S, Pasha M. Bayesian Spatiotemporal modeling for inverse problems. Stat Comput. 2023; 33.
11. Bacoyannis T, Ly B, Cedilnik N, Cochet H, Sermesant M. Deep learning formulation of electrocardiographic imaging integrating image and signal information with data-driven regularization. Europace. 2021;23(Supplement1):i55–62.
12. Alday EA, Colman MA, Langley P, Zhang H. Novel non-invasive algorithm to identify the origins of re-entry and ectopic foci in the Atria from 64-lead ECGs: A computational study. Plos Comput Biol. 2017;13(3):e1005270.
13. Biasi N, Seghetti P, Mercati M, Tognetti A. A smoothed boundary bidomain model for cardiac simulations in anatomically detailed geometries. PLoS ONE. 2023;18(6):e0286577.
14. Zhang Y, Adams J, Wang VY, Horwitz L, Tartibi M, Morgan AE, et al. A finite element model of the cardiac ventricles with coupled circulation: biventricular mesh generation with hexahedral elements, airbags and a functional mockup interface to the circulation. Comput Biol Med. 2021;137:104840.
15. Bai J, Lu Y, Zhu Y, Wang H, Yin D, Zhang H, et al. Understanding PITX2-dependent atrial fibrillation mechanisms through computational models. Int J Mol Sci. 2021;22(14):7681.
16. Yadan Z, Jian L, Jian W, Yifu L, Haiying L, Hairui L. An expert review of the inverse problem in electrocardiographic imaging for the non-invasive identification of atrial fibrillation drivers. Comput Methods Programs Biomed. 2023;240:107676.
17. Wang T, Karel J, Bonizzi P, Peeters RLM. Influence of the Tikhonov regularization parameter on the accuracy of the inverse problem in electrocardiography. Sensors. 2023;23(4):1841.
18. Bai Y, Chen W, Chen J, et al. Deep learning methods for solving linear inverse problems: research directions and paradigms. Signal Process. 2020;177:107729.
19. Sovilj S, Magjarević R, Lovell NH, Dokos S. A simplified 3D model of whole heart electrical activity and 12-Lead ECG generation. Comput Math Methods Med. 2013;1–10.
20. Ackerman MJ. The visible human project. Proc IEEE Inst Electr Electron Eng. 1998;86(3):504–11.
21. Gabriel S, Lau RW, Gabriel C. The dielectric properties of biological tissues: II. Measurements in the frequency range 10 hz to 20 ghz. Phys Med Biol. 1996;41(11):2251.
22. Rogers JM, Mcculloch AD. A collocation-Galerkin finite element model of cardiac action potential propagation. IEEE Trans Biomed Eng. 1994;41(8):743–57.
23. Karoui A, Bear L, Migerditichan P, Zemzemi N. Evaluation of fifteen algorithms for the resolution of the electrocardiography imaging inverse problem using ex-vivo and in-silico data. Front Physiol. 2018;9:1708.
24. Yao B, Yang H. Spatiotemporal regularization for inverse ECG modeling. IISE Trans Healthc Syst Eng. 2021;11(1):11–23.
25. Khan RA, Yang S, Fahad S, Khan SU. Kalimullah. A modified particle swarm optimization with a smart particle for inverse problems in electromagnetic devices. IEEE Access. 2021;9:99932–43.
26. Lecun Y, Bottou L, Bengio Y, Haffner P. Gradient-based learning applied to document recognition. Proc IEEE Inst Electr Electron Eng. 1998;86(11):2278–324.
27. Jyotishi D, Dandapat S. An LSTM-based model for person identification using ECG signal. IEEE Sens Lett. 2020;4(8):1–4.
28. Berger T, Fischer G, Pfeifer B, Modre R, Hanser F, Trieb T et al. Single-beat noninvasive imaging of cardiac electrophysiology of ventricular pre-excitation. J Am Coll Cardiol. 2006; 48(10).
29. Waller BF, Gering LE, Branyas NA, Slack JD. Anatomy, histology, and pathology of the cardiac conduction system: part II. Clin Cardiol. 1993;16(4):347–52.
30. Jæger KH, Trotter JD, Cai X, et al. Evaluating computational efforts and physiological resolution of mathematical models of cardiac tissue. Sci Rep. 2024;14(1):16954.

Publisher's note